

**ANALYTICAL AND EXPERIMENTAL RESULTS OF THE GROUND RESONANCE
PHENOMENON FOR A.129**

**ORLANDI/CERIOTTI/RUSSO
(DYNAMICS)
MARCHESE/MAINO/NAGARAJA
(ACOUSTICS AND VIBRATION)**

Engineering Department
COSTRUZIONI AERONAUTICHE G. AGUSTA
GALLARATE, ITALY

**TENTH EUROPEAN ROTORCRAFT FORUM
AUGUST 28 – 31, 1984 – THE HAGUE, THE NETHERLANDS**

ANALYTICAL AND EXPERIMENTAL RESULTS OF THE GROUND RESONANCE
PHENOMENON FOR A.129

ORLANDI/CERIOTTI/RUSSO
(DYNAMICS)
MARCHESE/MAINO/NAGARAJA
(ACOUSTICS AND VIBRATION)

Engineering Department
COSTRUZIONI AERONAUTICHE G. AGUSTA
GALLARATE, ITALY

ABSTRACT

This paper presents the methodology used in AGUSTA to investigate the Ground Resonance problem.

We deal with the three phases of the methodology, that are:

- design definition.
- analytical/experimental stage.
- ground resonance tests.

We emphasize the second phase, describing the ground vibration tests and their results for the experimental part, the two computer codes used with results and compares between them for the analytical part.

For the third phase we show the initial results of ground resonance tests and describe the way we analyze the signals obtained from these tests.

All the results and the data of the work are referred to the new AGUSTA 129 so they are not complete as the helicopter is still in the prototype phase.

2. INTRODUCTION

The well-known Ground Resonance problem is one of the major dangers that a new helicopter has to face, starting from its first flight.

A prototype that is affected by this type of dynamic instability could be destroyed in a glance, with evident problems to its crew and intolerable delays to its development.

To prevent this problem AGUSTA uses a methodology divided into three phases:

- design definition.
- analytical/experimental stage.
- ground resonance tests.

Each phase corresponds to a different period of the development of the project of the helicopter.

"the design definition" is devoted to define the typical components involved in the phenomenon (lag damper, landing gear, etc.) through a non-linear finite element model of the fuselage to take into account the geometry of the landing gear, its non-linear mechanic parameters and the stiffness distribution of the fuselage.

An example of this model is shown in fig. 1 in which we note that the fuselage is modelled by equivalent beams that take into account the whole deformability of the structure, while for the undercarriage we use nonlinear beams simulating the nonlinear shock strut characteristics.

The great advantage of using a finite element model is, of course, that it can be described with any desired degree of sophistication.

With this model we find the static deformation of the machine, with and without airborne (typical values of airborne used in our analysis are: 25%, 50%, 75%, 90%) and, for these conditions, we determine natural frequencies and their generalized modal parameters. Fig. 1 shows a roll mode of the helicopter without airborne.

These outputs are then utilized in a FORTRAN code named 'G.RE.CA.' (Ground Resonance Calculus), based on the "FLOQUET THEORY" in which each rigid blade may be described separately with its own characteristics.

In this way it is possible to simulate single blade damper failures and to define an acceptable range of values for each blade parameter.

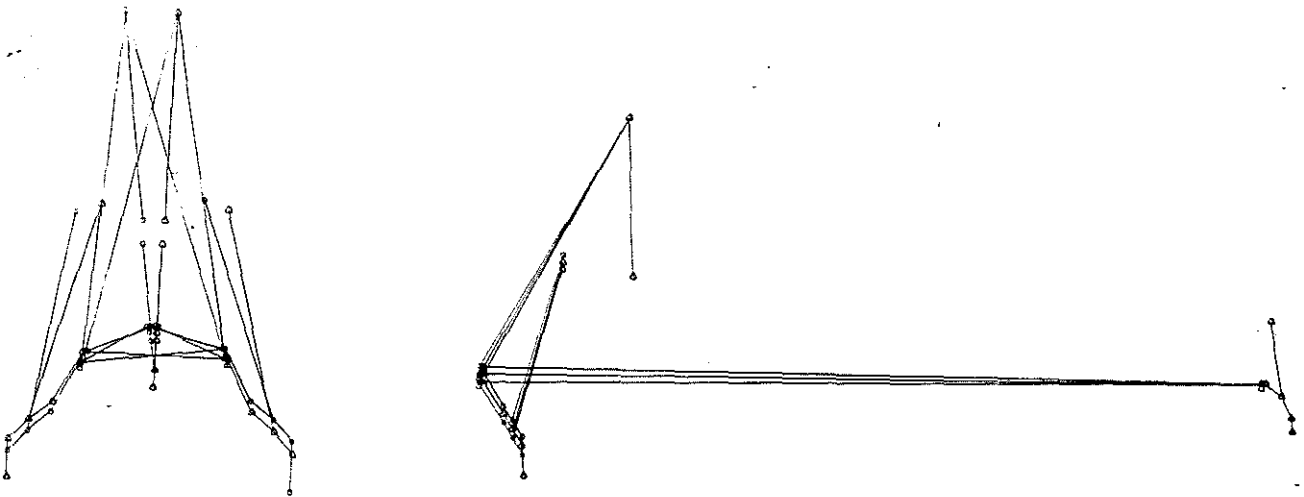
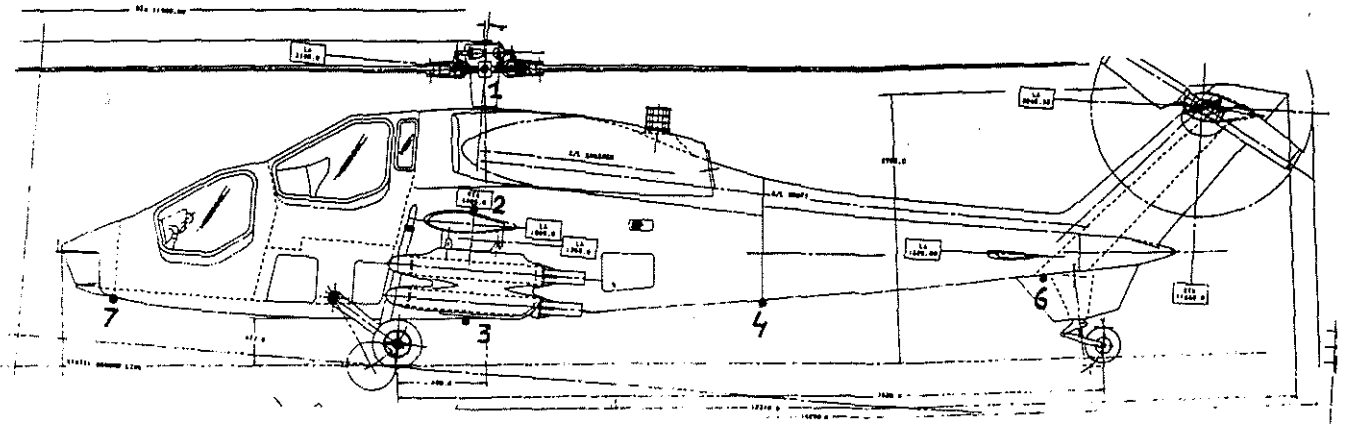


Fig. 1 Ground resonance finite element model for A129.

The regions with reduced stability are then investigated by a General Rotorcraft Dynamic Program (G.R.D.P.), developed in AGUSTA, able to consider all the aerodynamic aspects and degrees of freedom of blades and fuselage. The effect of thrust, gyroscopic moments and dynamic inflow are so introduced to refine the results obtained from the previous analyses.

The "analytical/experimental stage" provides an opportunity to consolidate the analytical studies: the analytical modes and generalized parameters are substituted by the experimental ones, obtained from ground vibration tests on the first prototype. These tests cover the whole weight and c.g. envelope for different airborne states of the helicopter. In this way, before test flights, we can be sure that the physical description of the machine is correct as to improve the prediction of the Ground Resonance behaviour.

Fig. 2 is a photograph of one of the first test flights of the A.129.



Fig. 2 A129: one of the first test flights.

Finally "ground resonance tests" are performed on the flight machine by applying different perturbations to the controls.

These tests are performed at different airborne states at nominal RPM and, without airborne, at different RPM over different types of ground (concrete, grass etc.)

From these tests we obtain frequencies and corresponding damping levels to satisfy the certification procedures, and to compare with the results obtained from the analyses of phase two.

In fig. 3 we give a summary of the methodology, describing the major details for each phase.

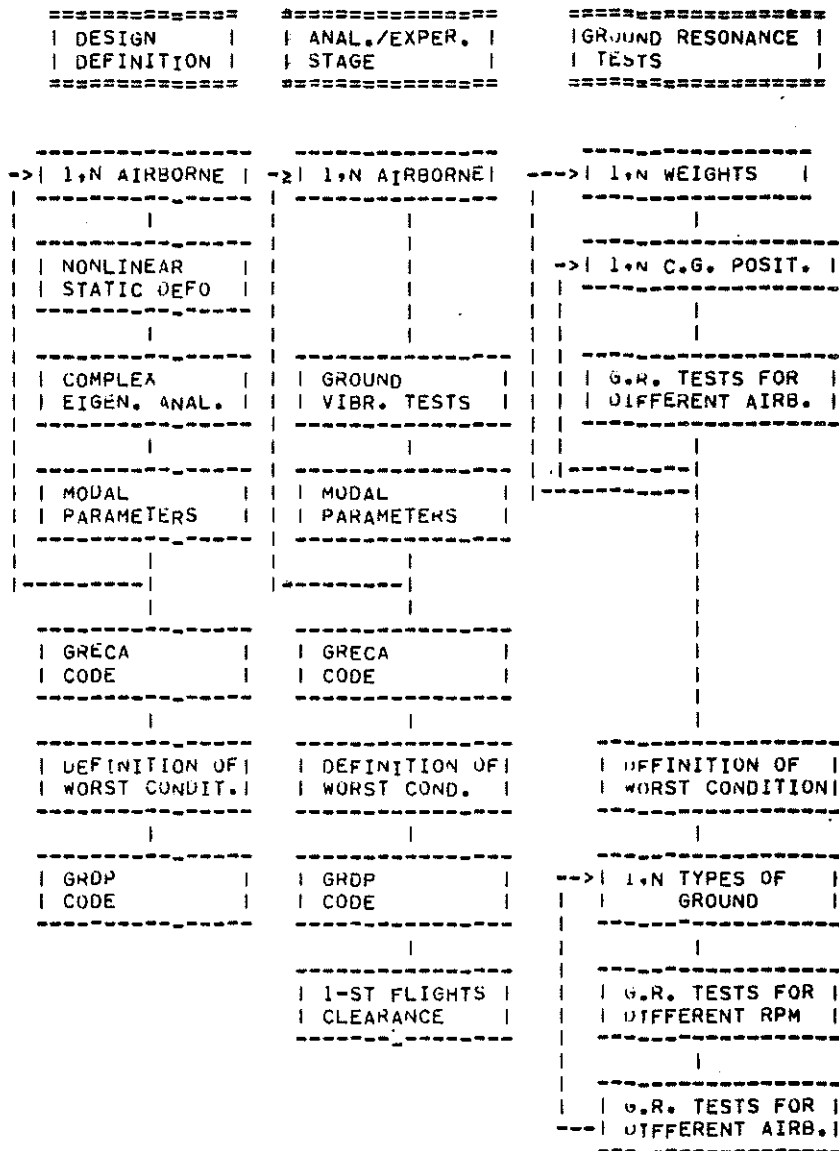


Fig. 3 Flow chart of Ground Resonance Methodology..

2. ANALYTICAL THEORY

The analytical part of the work has been carried out with the help of two computer codes: 'GRECA' and 'GRDP'.

- The code GRECA is dedicated to the Ground Resonance problem and involves the following degrees of freedom: for the rotor, the rotation about the drag hinge of each blade and, for the fuselage, some mode shapes of lowest frequency of a grounded helicopter (see fig. 4). The method consists in writing the linearized equations of motion with periodic coefficients (see Appendix A) and in determining a Transition Matrix over a period equal to that of the periodic coefficients, that is the period of revolution. According to the Floquet theory (ref. 1) an eigenvalue analysis is then performed on this matrix: if the real part of the eigenvalues obtained is negative the system is stable, otherwise the system is unstable. The method of integration used is a Peano method (Appendix B) that we found more effective than the Runge-Kutta of fourth order previously used. To improve the results obtained with the linearized code, the GRDP nonlinear program, based on a finite element technique, is used for the most critic cases previously found. We can so take into account aerodynamic aspects, neglect linearization and check the effects of further degrees of freedom for blades and fuselage.

Fig. 5 is an example of the Ground Resonance GRDP scheme for the A.129.

The GRDP theory is largely described in Ref. 2.

3. EXPERIMENTAL DETAILS

The experimental tests were carried out in our Vibration Laboratory.

The data acquisition and signal analysis were made through a GENRAD system that uses the software DATM and MODAL PLUS of SDRC (ref. 4).

The airborne was simulated with an overhead travelling crane connected to a tool with belts joined to the mast of the helicopter. The presence of a load cell gave us the airborne value (see fig. 6).

A flow chart of the test rig is showed in fig. 7.

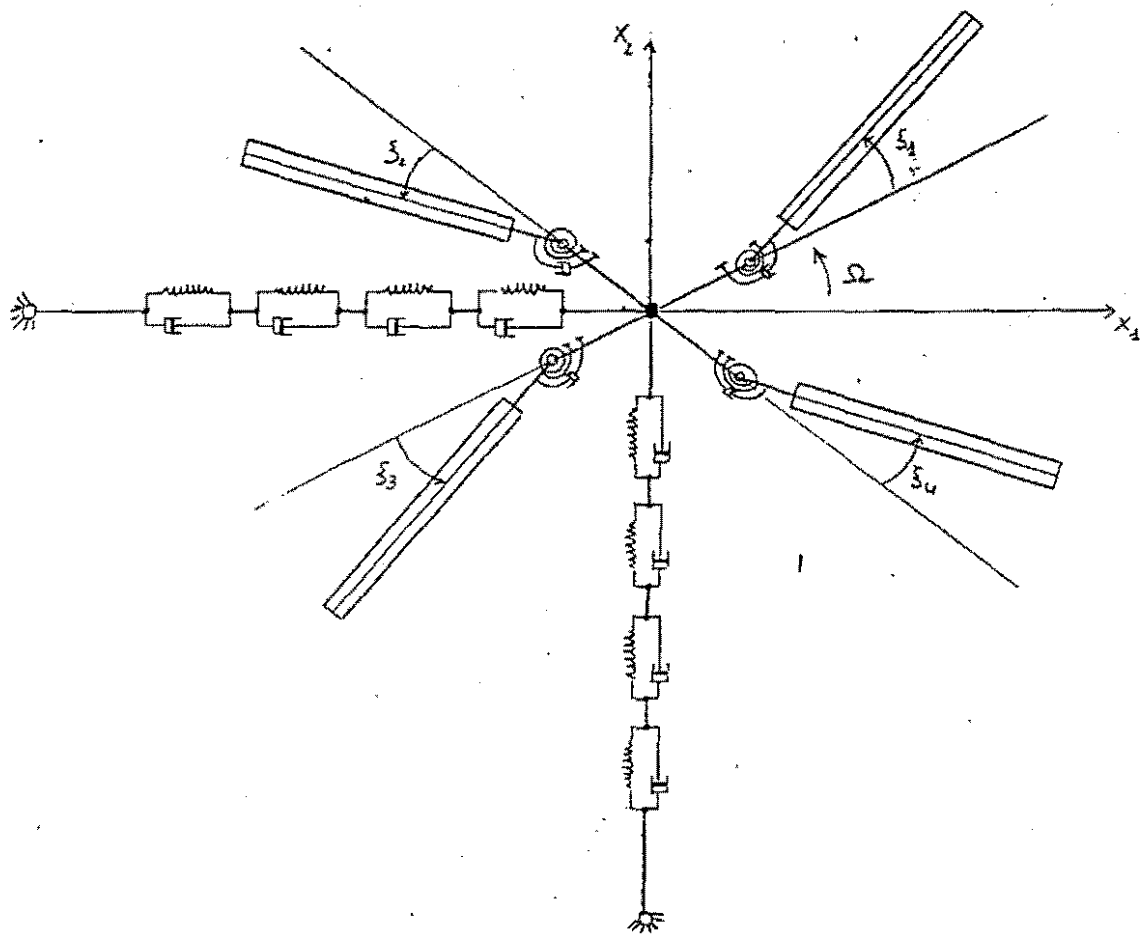


Fig. 4 Ground resonance GRECA scheme.

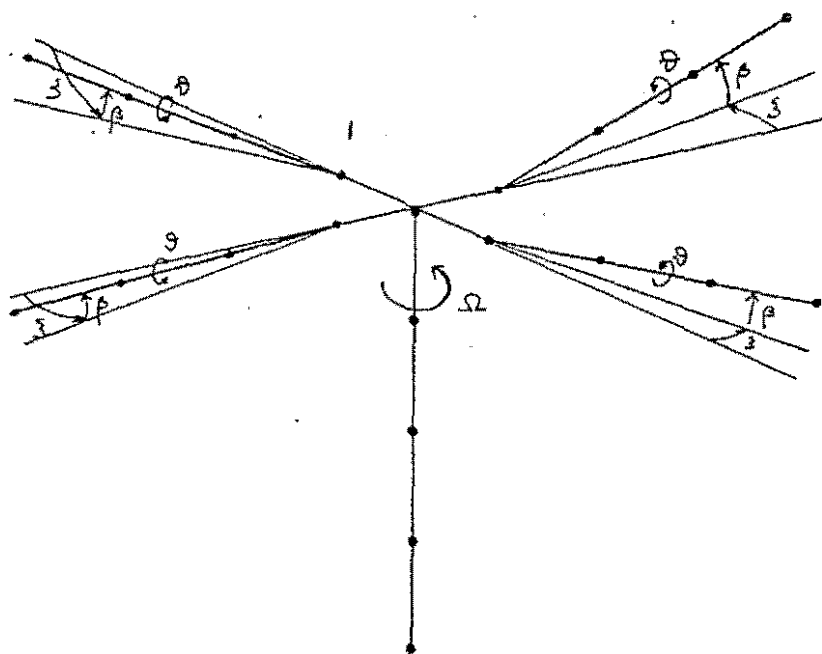


Fig. 5 Ground resonance GRDP scheme.

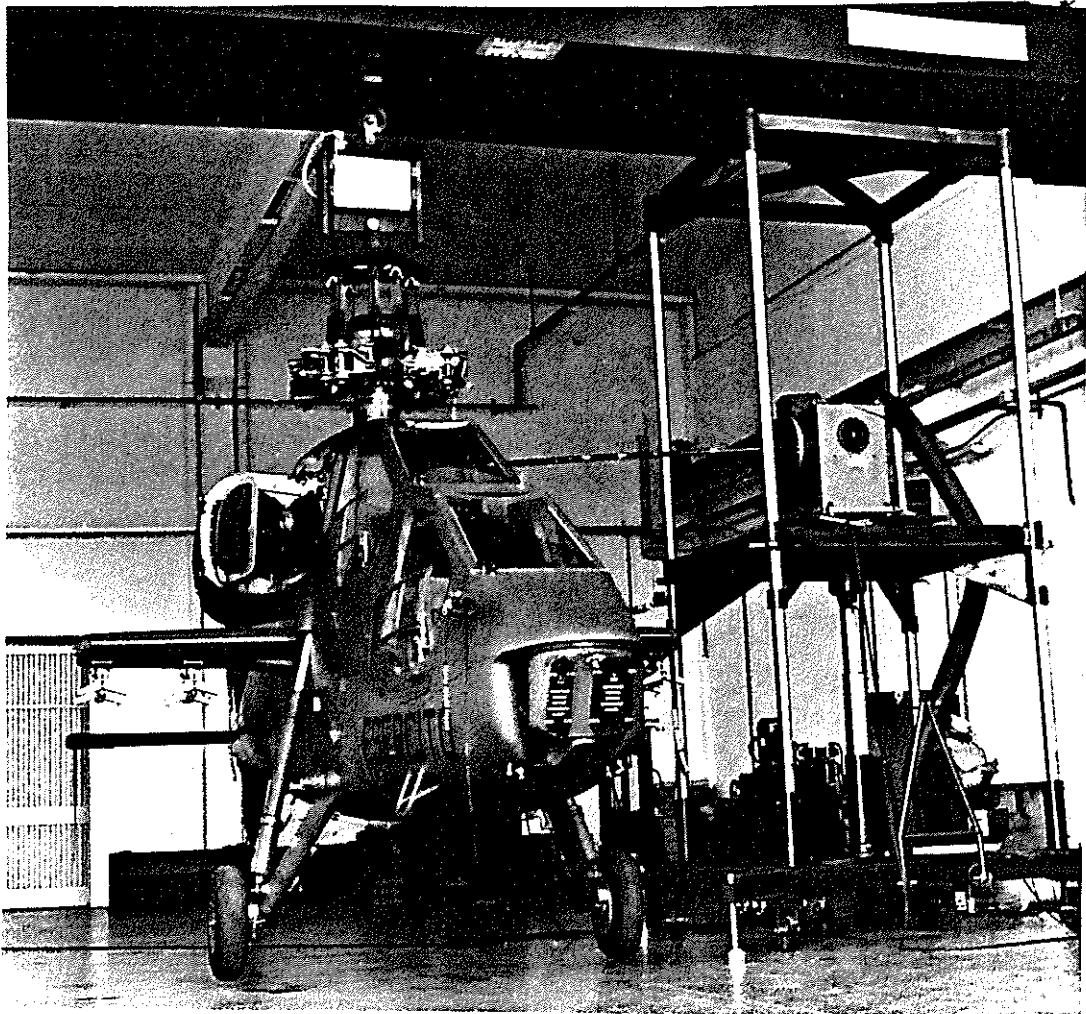


Fig. 6 Al29 during ground vibration tests.

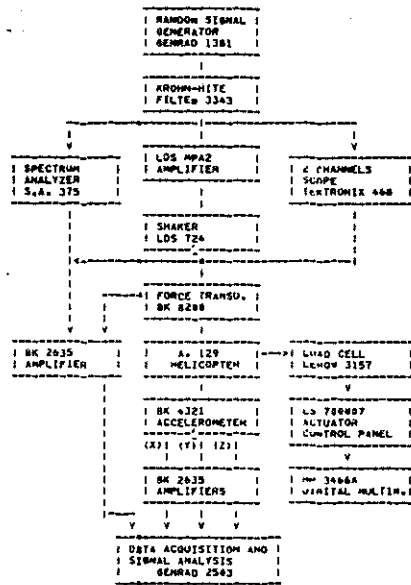


Fig. 7 Flow chart of the test rig.

Preliminary tests made to determine the best kind of excitation showed that the random excitation allowed us to attain more significant results.

In order to obtain accurate modal parameters and shapes, the excitation force amplitude should be constant in the whole frequency range of interest. Due to the dynamic behaviour of the excitation system, we met troubles in obtaining good excitation force level at low frequencies (below 15 Hz). Therefore we had to increase the amplitude of the drive signal in the range above specified. To this aim a lowpass 20 dB gain filter was employed. In this way a better signal to noise ratio and consequently an higher coherence value was achieved.

Fig. 8 shows the low frequency amplified drive signal and the actual excitation force signal as picked up by the force transducer which connects the excitation beam tip to the mast.

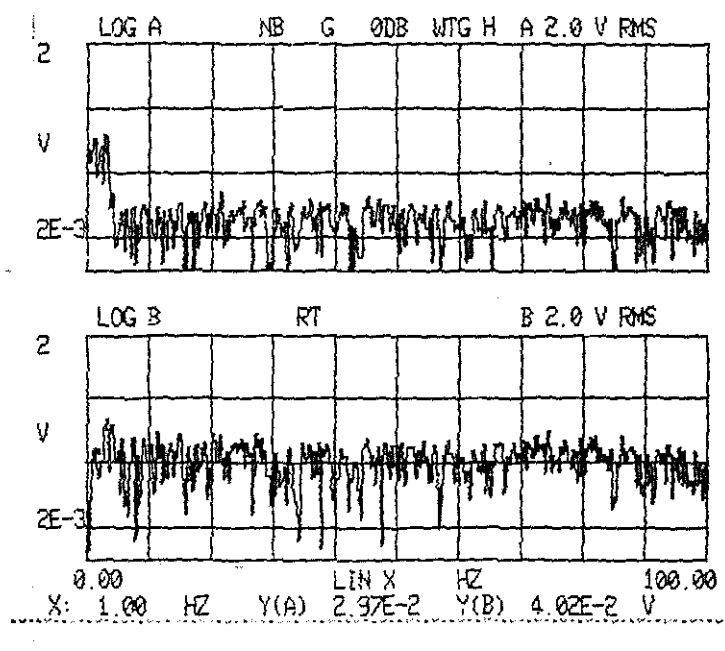


Fig. 8 Comparison between drive signal (upper) and excitation force signal (lower).

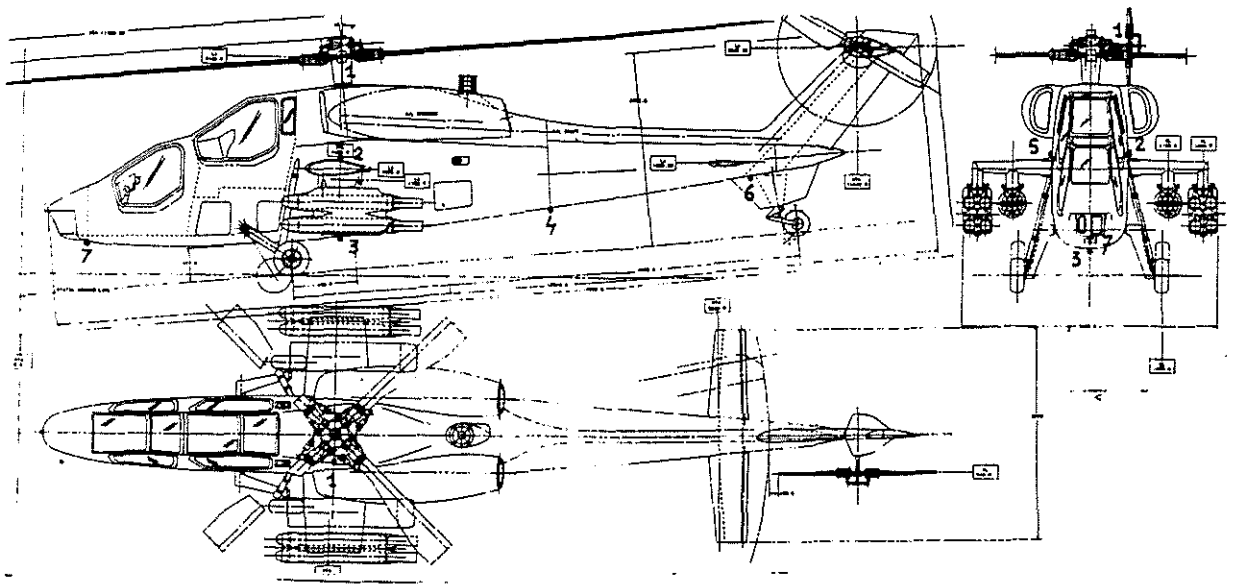


Fig. 9 Position of the accelerometers for ground vibration tests.

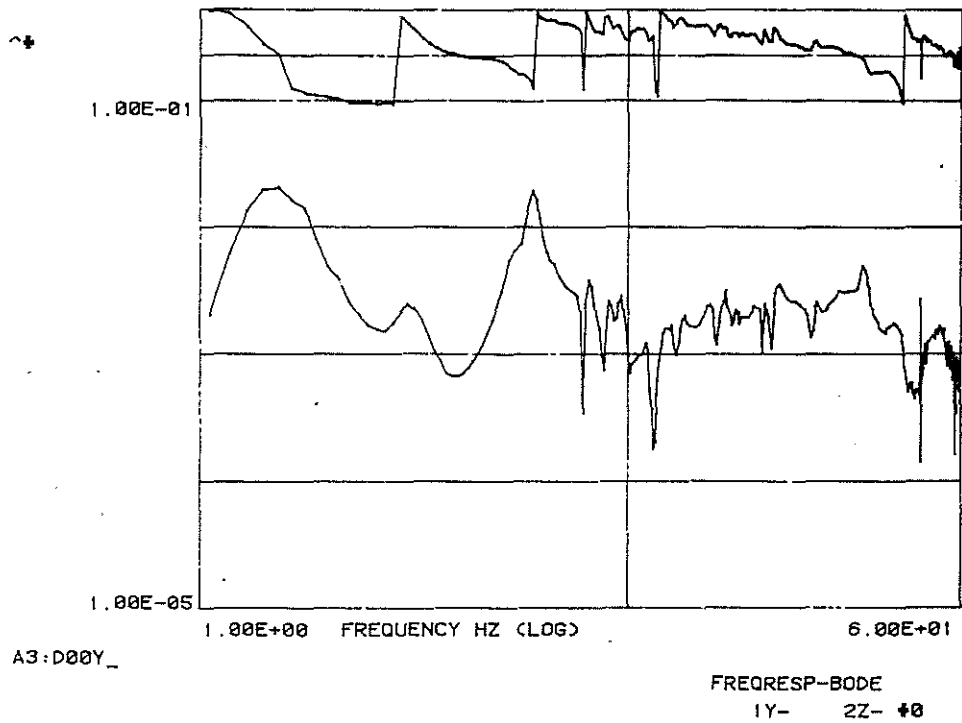


Fig. 10 Typical transfer function for ground vibration tests.

The DATM software builds a transfer function between the signal of an accelerometer and the signal of the force transducer (see fig. 10) after having made a sampling of the signal and a Fast Fourier Transform.

Fig. 9 shows the position of the accelerometers used on the helicopter; the following table gives the data acquisition characteristics:

! Trigger type	free-running	! Excitation	RANDOM	!
! Coupling code	DC	! Overlap factor	4	!
! Weighting code	HANNING	! Sampling freq. (HZ)	160	!
! Ensemble size	40	! Resolution (HZ)	0.15	!
! Max frequency (HZ)	40	! Sample length (sec)	6.30	!
! A-A filters (HZ)	60	!		!

The signal analysis, starting from an analytical model of the transfer function, computes the natural frequencies, the modal damping, the amplitude and phase of the residual according to the following formulae:

$$H_{ik}^r(s) = \frac{x_i(s)}{F_k(s)} = \sum_{r=1}^N \frac{A_{ik}^r}{s-s_r} + \frac{A_{ik}^{r*}}{s-s_r^*}$$

where:

H_{ik}^r = transfer function measured at the point "i" (response) when excitation is at the point "k" (reference)

A_{ik}^r = amplitude of the residual for the "r" mode

A_{ik}^{r*} = conjugate complex of A_{ik}^r

$s = \zeta + i \omega$ Laplace variable

$s_r = \zeta_r + i \omega_r$ where ω_r is the natural frequency of the "r" mode

s_r^* = conjugate complex of s_r

N = number of the modes

From the natural frequencies and through a curve-fitting technique, the mode shapes are calculated.

Then, through the MASS computing program, modal mass, damping and stiffness are computed normalized with respect to the reference point.

The expression of the modal mass is:

$$m_r = \left| \frac{\frac{\psi_i^r \psi_k^r}{(\alpha_i^r)^2}}{2 \omega_r A_{ik}^r} \right|$$

where:

$$\alpha_i^r = \psi_{\text{reference}}^r = \psi_k^r \quad (\text{because it is normalized to the reference point})$$

ψ_i^r = modal displacement at the response point

ψ_k^r = modal displacement at the reference point

ω_r = natural frequency

A_{ik} = amplitude of the residual

while the expression of the stiffness is:

$$k_r = (\zeta_r^2 + \omega_r^2) * m_r$$

where:

$$\zeta_r = \zeta_r \omega_{r,n}$$

ζ = damping rate

$\omega_{r,n}$ = natural frequency without damping

4. FLIGHT TEST PROCEDURE

Flight tests are performed to verify that the helicopter is really safe from Ground Resonance and that all the analytical and experimental previsions are good.

The tests are performed by giving a perturbation to the rotor through the cyclic pitch, recording the responses of some accelerometers on the machine and analysing these signals.

The kind of perturbation, illustrated in fig. 11, is a counterrotorwise motion of the cyclic pitch stick at a frequency of about $2/3$ per Rev.

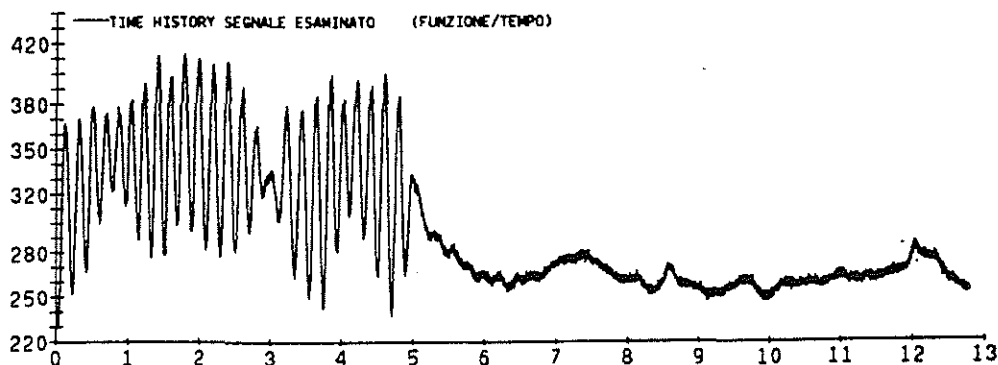
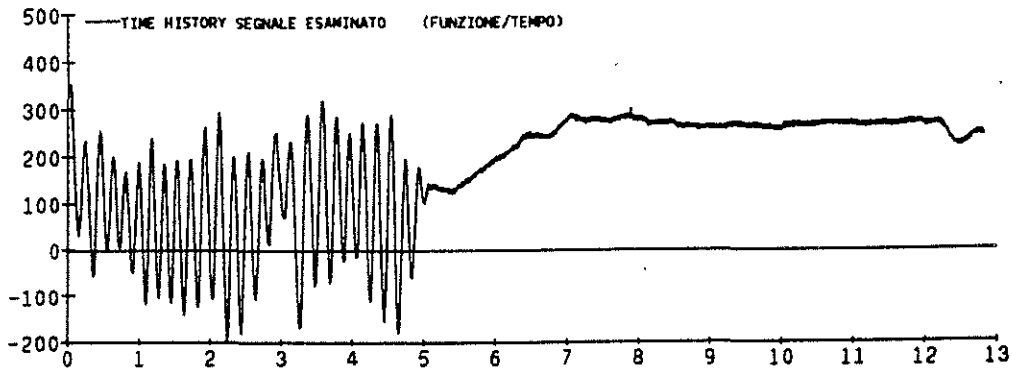


Fig. 11 Cyclic pitch stick motion: lateral (upper) and longitudinal (lower)

This perturbation is maintained until a good response of the machine is achieved, after which the cyclic input is stopped in the neutral position and the recording goes on for 10/15 seconds with a sample rate of 1000 points/Rev.

The signals chosen for analysis are taken from a chord bending strain and a damper displacement for the rotor, a non-rotating accelerometer on the top and inside the mast for the fuselage.

Fig. 12A , 12B show these signals without and with a lowpass filter at 25 HZ.

These recordings are made at different percentage of nominal RPM and at different percentage of collective pitch:

! Flight no.	! % RPM	! % AIRBORNE	!
! 37/8	! 98	! 0	!
! 37/11	! 102	! 0	!
! 40/16	! 100	! 57	!
! 40/21	! 100	! 76	!

A moving-block analysis (Ref. 3) is then performed: starting from the end of the input perturbation we compute the value and the damping of all the frequencies contained in the signal from 0 to 20 HZ. Then we perform a more accurate analysis of those frequencies near to the natural lag mode and of those that seem to be undamped, with the exception of the forcing ones.

This work is done with the help of an interactive graphic program with which it is possible to select the time period of analysis, to use digital filters of different orders and windowing (Hanning), to select the block length for best optimization, to choose a Discrete of Fast Fourier Transform and to define the range of the moving-block function in which we want to compute the damping of the examined frequency; so, through the moving-block function, it is possible to follow the damping time-history of the examined frequency.

Fig. 13 illustrates an output of this program for the case F.

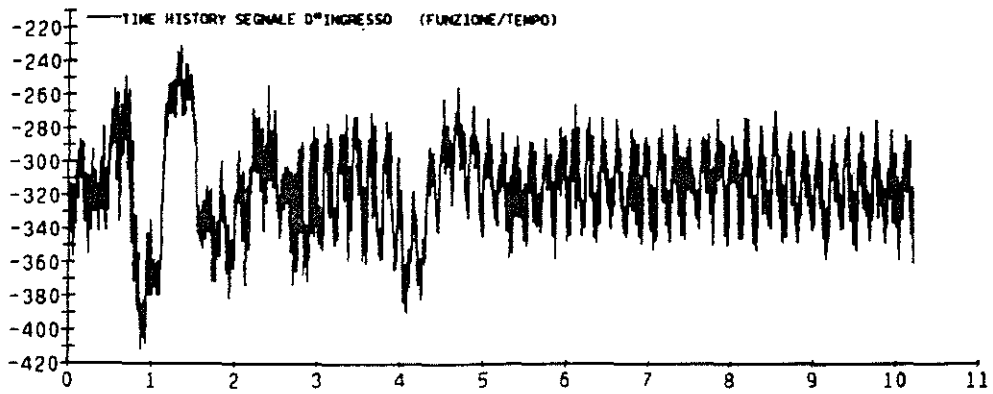
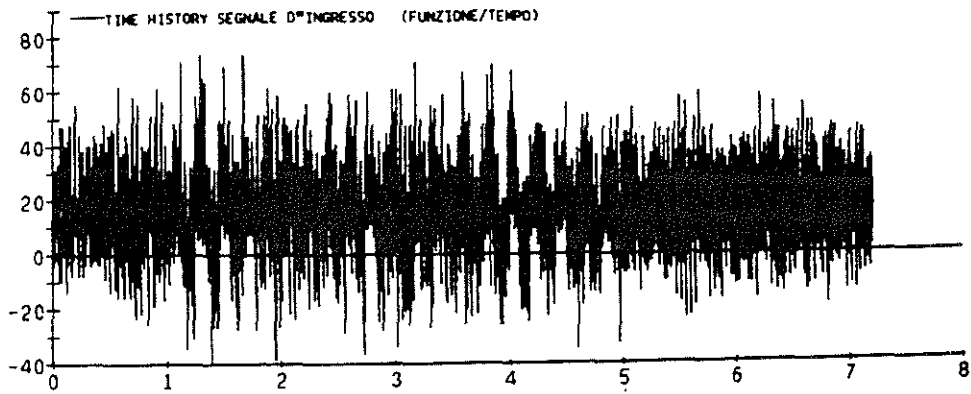
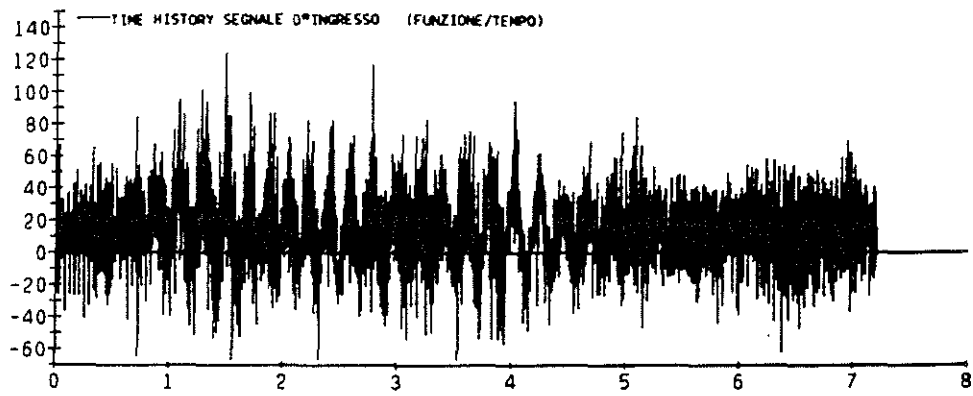


Fig. 12A Longitudinal, lateral hub and blade damper displacement: no-filtered signals.

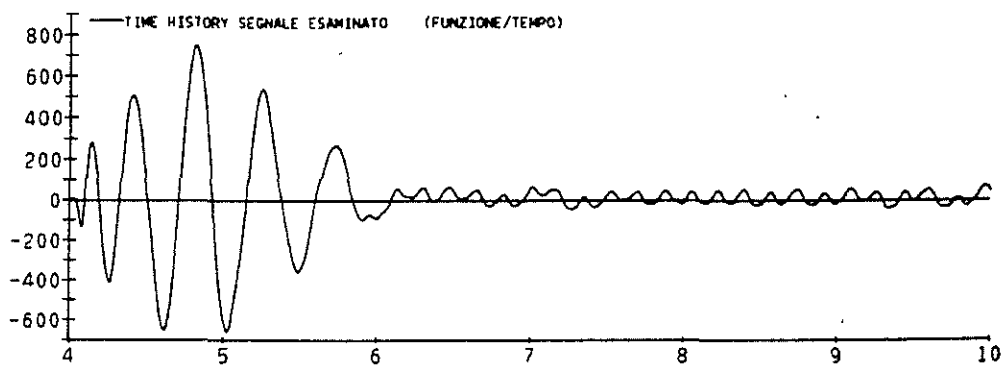
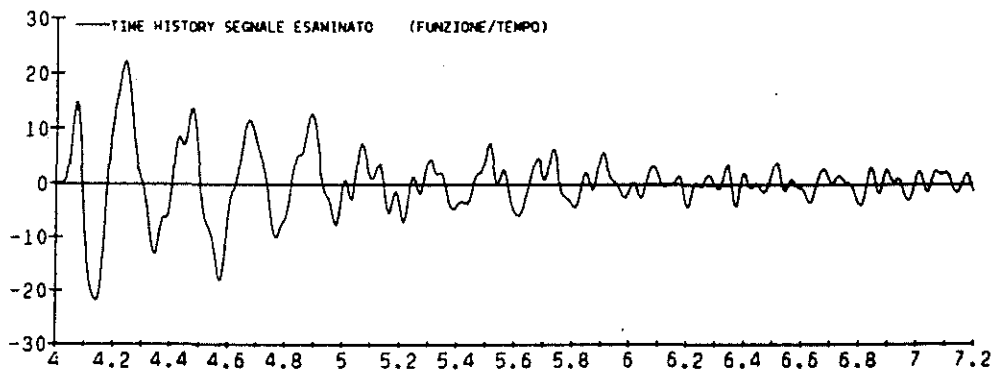
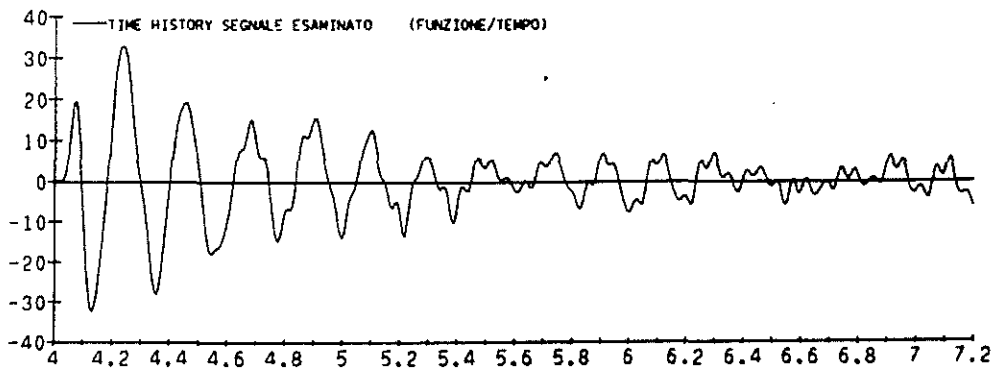
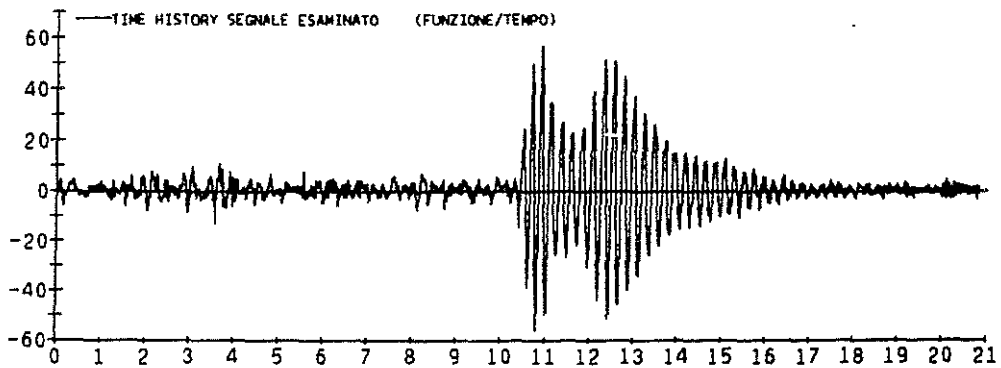
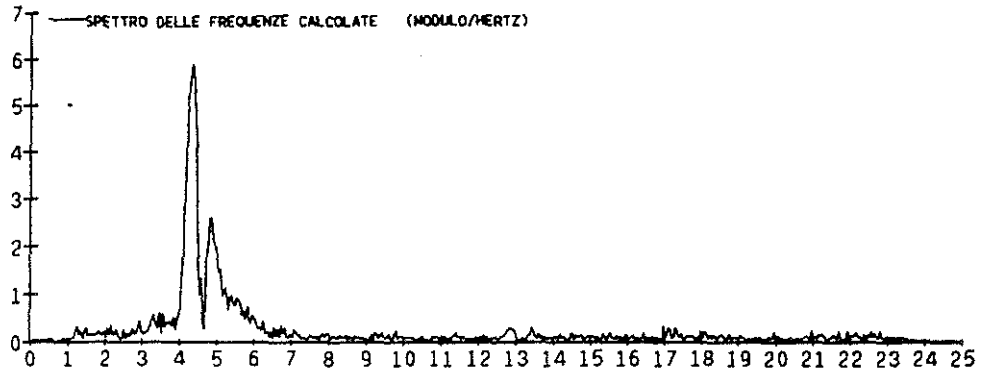
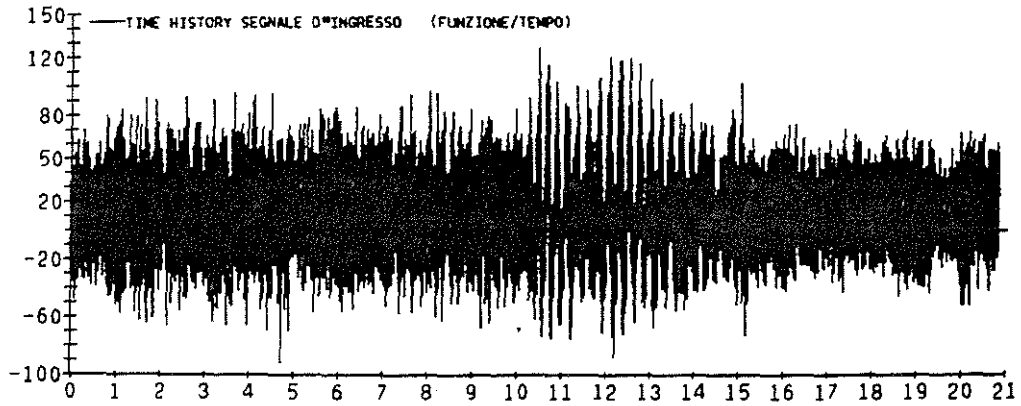


Fig. 12B Longitudinal, lateral hub and blade damper displacement: filtered (0-25 Hz) signals.



ANALISI MOVING-BLOCK

FREQUENZA N. 9 (HZ) = 7.1429
 AMPIEZZA (USER-UNITY) = 0.4679
 SMORZAMENTO (C/CCRIT) = -0.0103
 HALVING TIME (SEC) = 1.4953
 LUNGH. BLOCCO (P.TI) = 1750
 LUNGH. SEGNALE (P.TI) = 3501

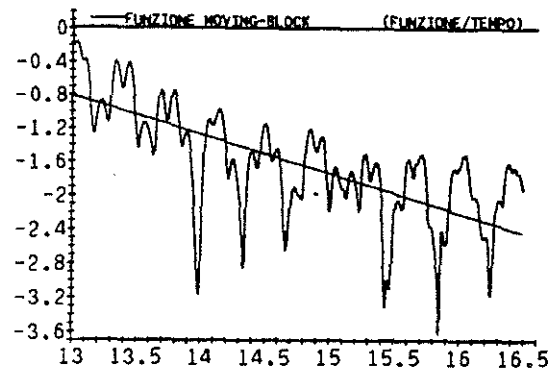


Fig. 13 Typical MOVING-BLOCK program output.

5.0 RESULTS

The shown results are given according to the following values of weight and C.G. position:

! Case !	Weight (kg) !	C.G. Pos. !	% Airborne !
! D !	3090 !	Neutral !	0,25,50,70,75,90 !
! F !	3273 !	Neutral !	0,25,60,75,87 !
! G !	3728 !	Neutral !	0,25,60,75,90 !

5.1 GROUND VIBRATION TESTS RESULTS

The results of the ground vibration tests are the modal parameters of the natural frequencies found (see appendix A) : we used the modal mass, damping and stiffness of the frequencies found between 0 and 25 Hz as input for the GRECA code.

In the following table there are these modal values for the case F , 0% airboirne:

! Mode !	freq. (Hz) !	modal mass (kg) !	modal_damp. (Nm ⁻¹ s) !	modal_stiff. (Nm ⁻¹) !
! 1 !	5.89 !	1196.4 !	1729.5 !	1639800. !
! 2 !	6.72 !	2984.1 !	10729.0 !	5340700. !
! 3 !	8.37 !	67044.0 !	136290.0 !	185550000. !
! 4 !	15.53 !	118720.0 !	426280.0 !	1130900000. !

5.2 GRECA CODE RESULTS

The results of the GRECA code are shown as plots -C/Ccrit vs. %RPM or %AIRBORNE, thus simulating the condition of starting/switching off the rotor and taking off/landing of the helicopter.

In Fig. 14 we see the plot of -C/Ccrit of each eigenvalue extracted from the Floquet Transition Matrix vs. %RPM . In this plot the numbers stand for the number of the mode found in the ground vibration test, while letter B stands for the

mode related to the blades. There is a difficulty in connecting the right modes as the order of the extraction of the eigenvalues is random, so we had to run our code eliminating each mode one at a time, as to join each eigenvalue to its related mode.

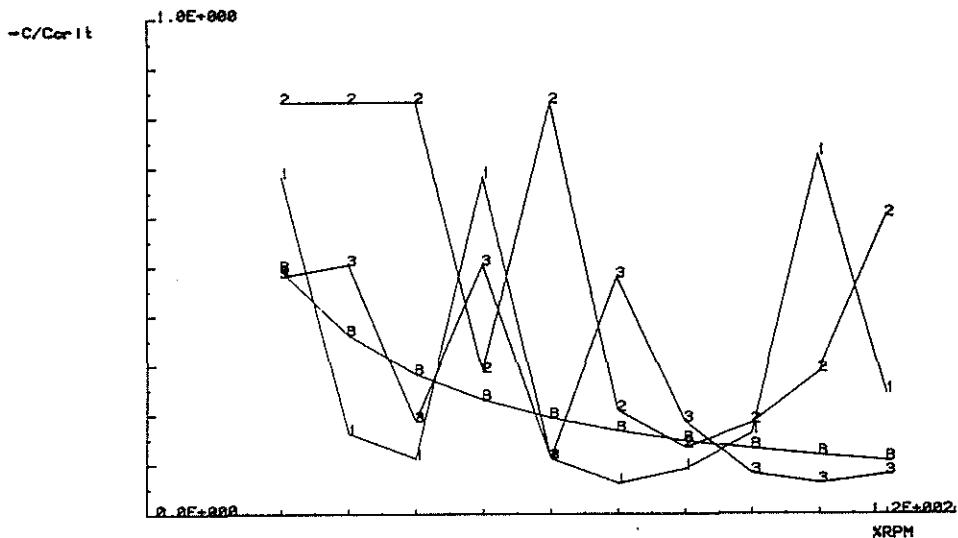


Fig. 14 GRECA results: $-C/C_{crit}$ vs. X RPM (case F)

The strange behaviour of the fuselage modes suggests further investigation of the phenomenon.

Fig. 15 is a $-C/C_{crit}$ vs. %AIRBORNE plot. In this plot the difficulty of connecting the right modes is due to the fact that they come from tests executed at different conditions of airborne. So the frequency of each mode vary, a mode can disappear and a new one can appear. For this reason we had to compare the mode shapes of the frequencies of comparing values and to connect between them the most similar ones.

In fig. 16 we plot, for the three different weight conditions D, F, G, the maximum value of the halving time that corresponds to the the lowest stability value. From the plot we note how there is a general decrease of stability around 70-75 %AIRBORNE and then a new increase.

5.3 GRDP RESULTS

The GRDP has been run during the design-definition phase, using as fuselage characteristics equivalent mass, damping and stiffness matrix from a finite element program (NASTRAN). In fig. 18 we show longitudinal (X) and lateral (Y) displacement of the hub and the pitch motion of the blades obtained from this analysis.

We are working on the GRDP input to accept the modal parameters from the ground vibration tests as fuselage characteristics; in this way it will be possible to use it also for phase two of our methodology.

5.4 FLIGHT TESTS RESULTS

As the results of the FLOQUET METHOD are related to the envelope of the actual signal (see appendix B) we preferred to compare the flight test results to a time-history generated by the same GRECA code.

The results of a moving-block analysis of the GRECA time histories are summarized in tab. 1, while in tab. 2 and 3 there is the comparison between analytical and flight test results for 0% and 75 %AIRBORNE.

The last two tables contain the most interesting frequencies of the two signals and the associated damping and halving time. The same results are plotted in figg. 17A, B, C for the hub lateral and longitudinal motion and blade drag motion.

These results, although first from a set of planned Ground Resonance flight tests, show a satisfactory agreement with our analytical predictions. Some frequencies and the related damping are well correlated while other, as for example in tab. 2 for the longitudinal hub are more shifted but its damping is still comparable.

We are still working on the flight tests to define the best way of excitation as to improve the content of information of the signal like low frequency spectrum, damping behaviour etc., and to improve the signal analysis.

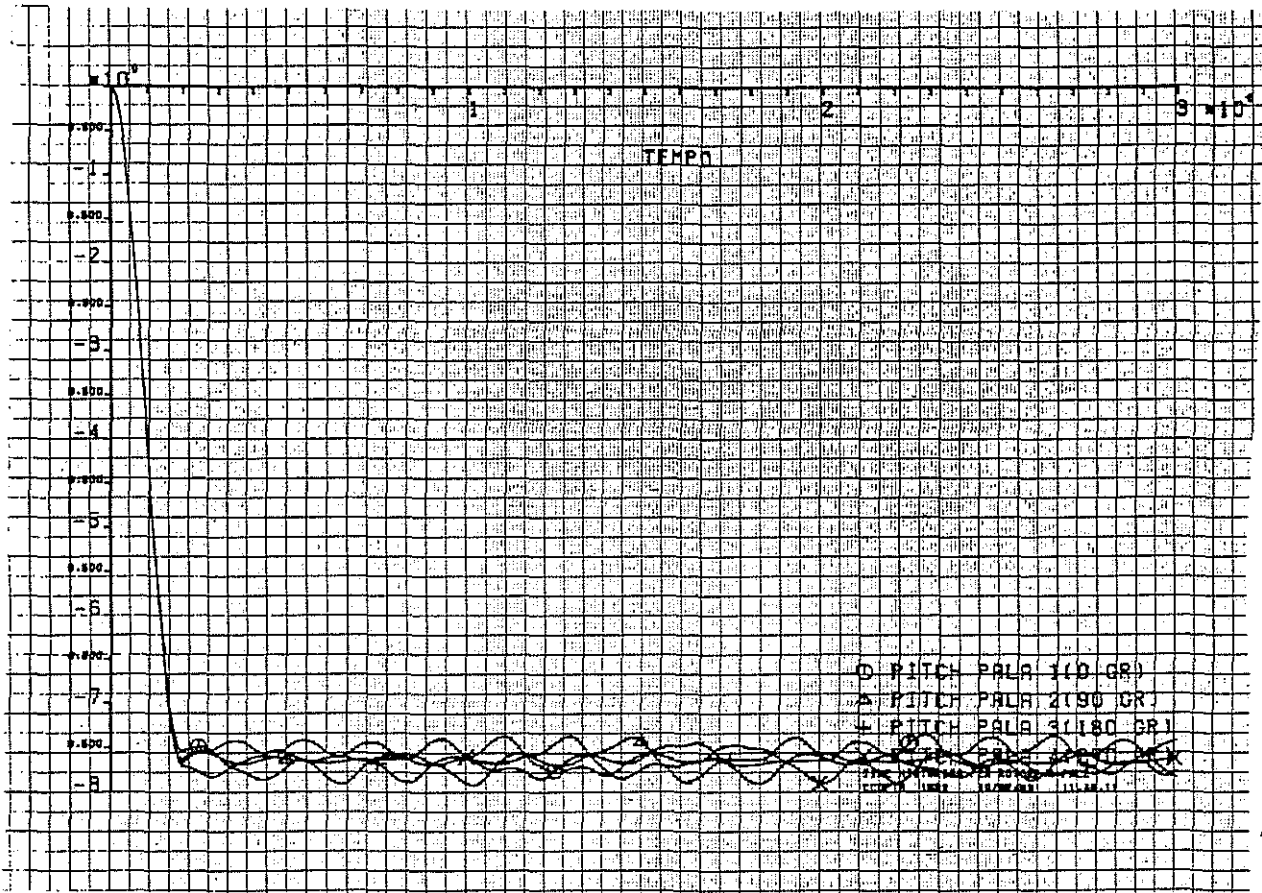
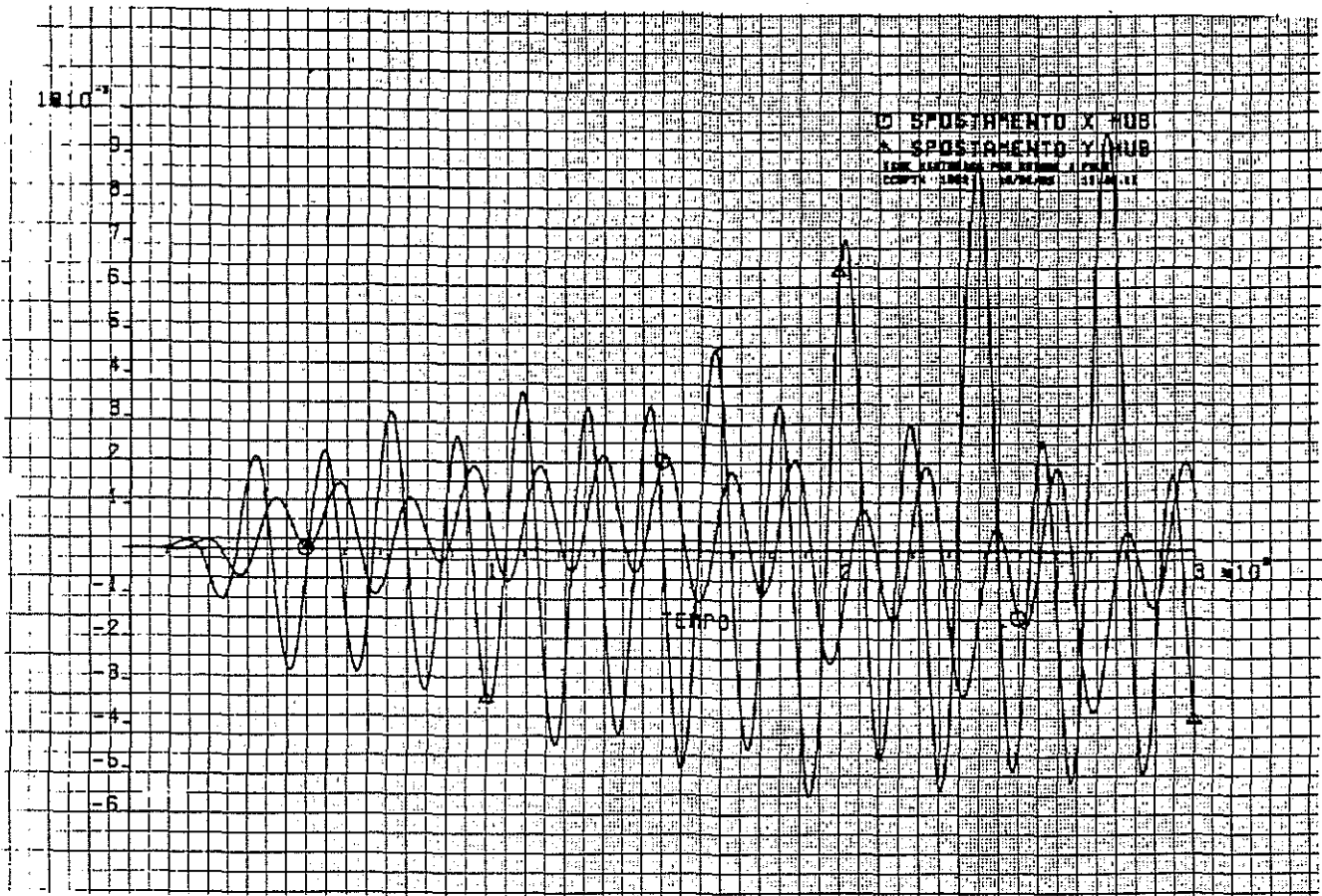


Fig. 18 GRDP results. Longitudinal and lateral hub displacement (upper) and pitch command (lower)

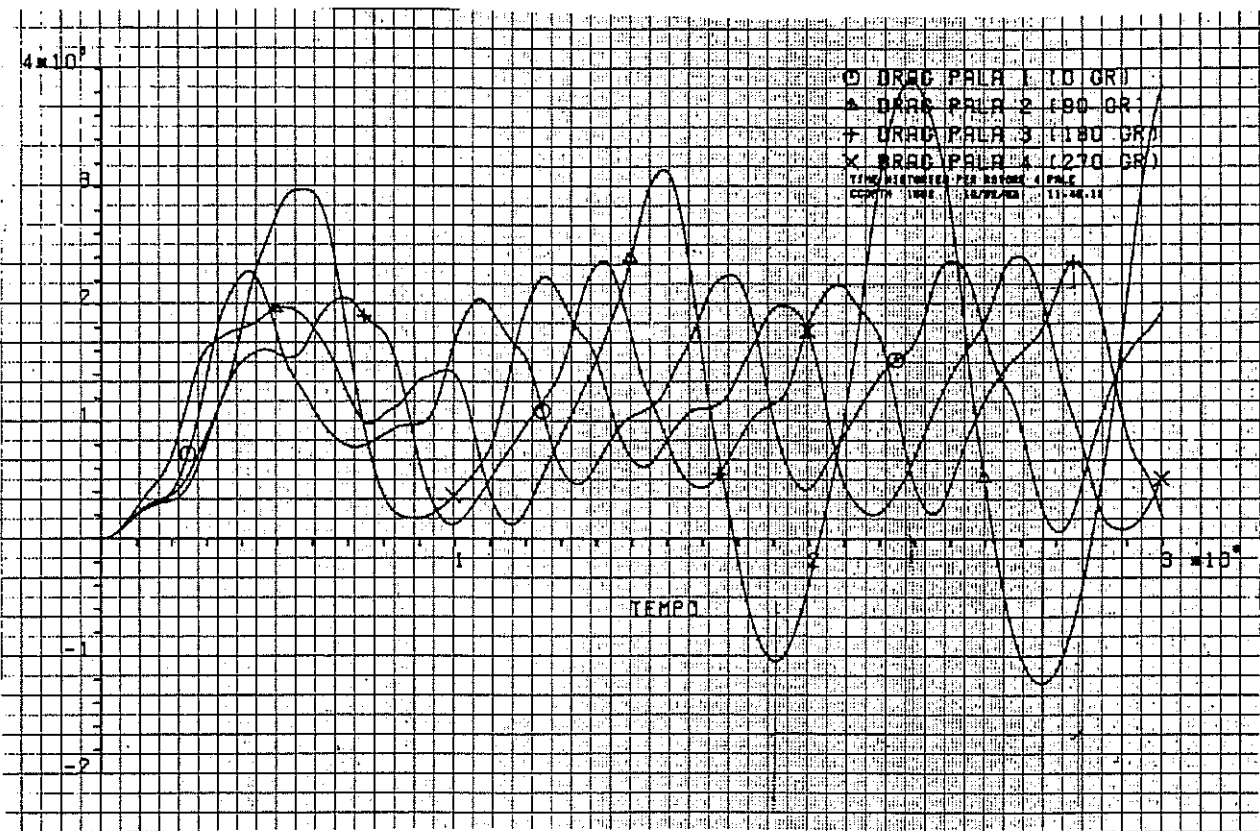
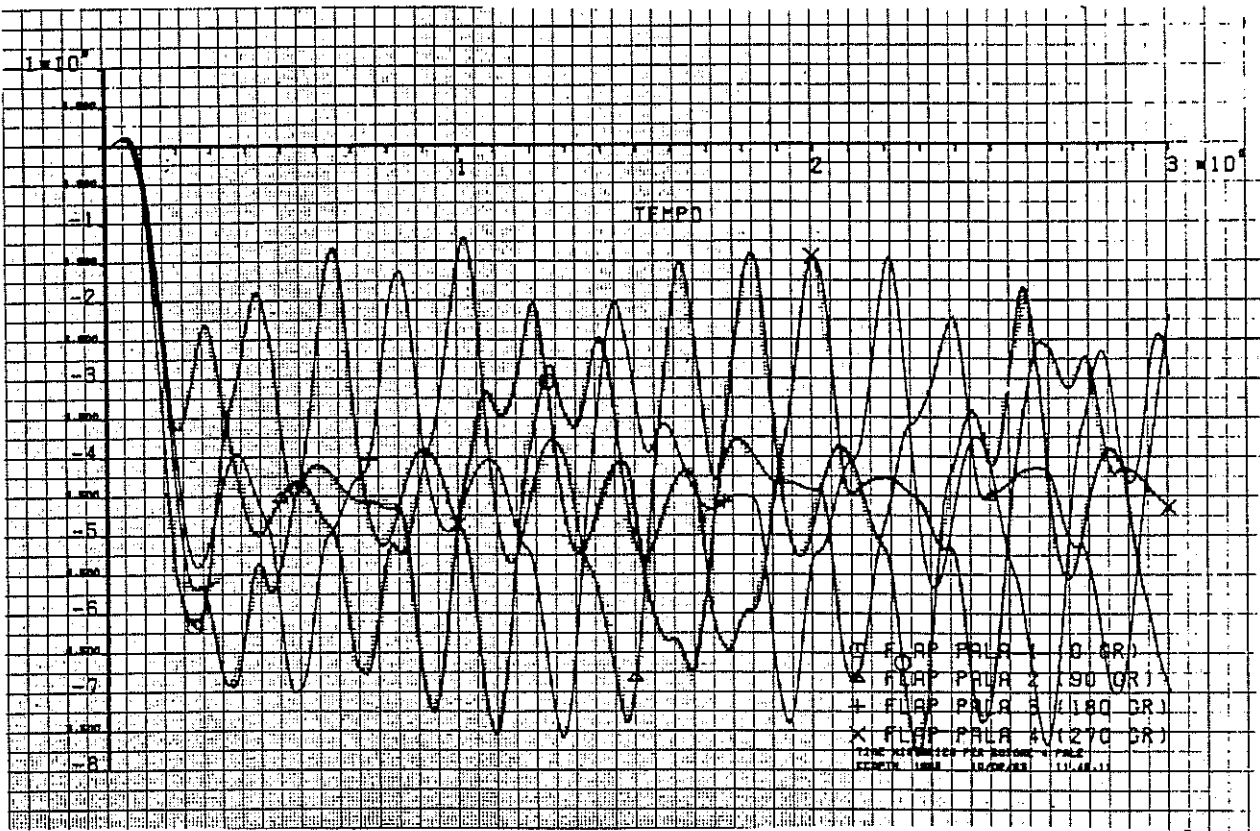


Fig. 19 GRDP results. Flap motion (upper) and drag motion (lower) for main rotor blades.

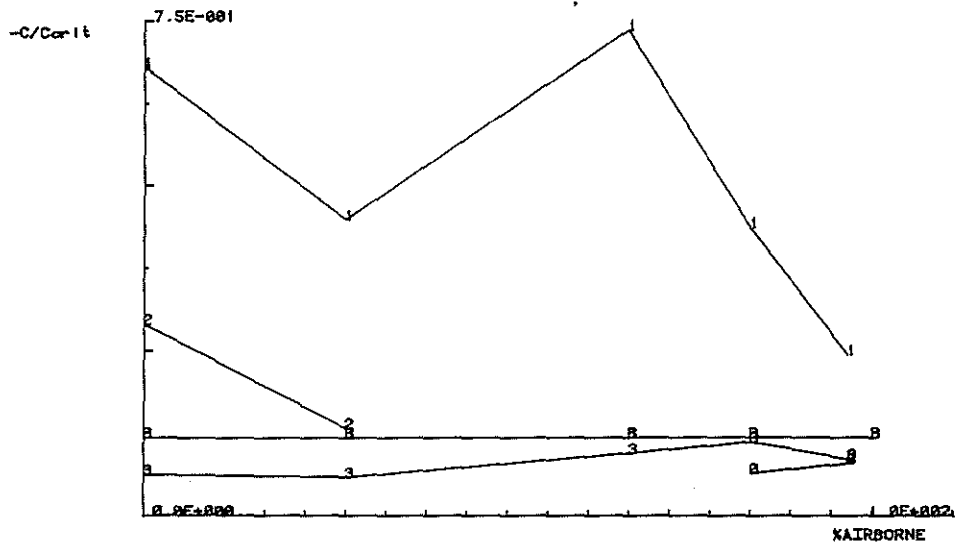


Fig. 15 GRECA results: -C/Ccrit vs. %AIRBORNE (case F)

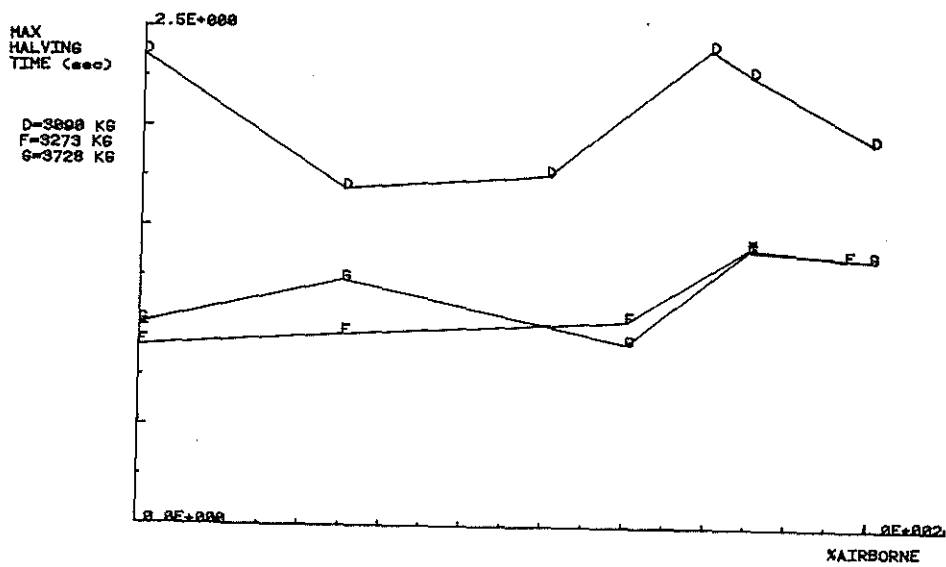


Fig. 16 GRECA results: MAX HALVING TIME vs. %AIRBORNE for different weights

% airborne	0%			25%			60%			75%			87%		
	Hz	c/cr	T/2	Hz	c/cr	T/2	Hz	c/cr	T/2	Hz	c/cr	T/2	Hz	c/cr	T/2
LATERAL HUB	3.91	-.056	0.504				4.18	-.052	0.505				4.12	-.020	1.342
				6.18	-.020	0.882				5.36	-.027	0.759			
	7.34	-.028	0.528				7.61	-.027	0.536	7.47	-.015	0.966	6.09	-.013	1.354
						20.30	-.012	0.441				7.49	-.013	1.143	
												21.34	-.004	1.259	
LONGITUDINAL HUB	3.91	-.035	0.800							4.54	-.017	1.437	4.64	-.019	1.227
				5.55	-.021	0.959									
	5.90	-.019	0.956	6.16	-.021	0.874	5.87	-.018	1.034	5.99	-.018	0.995			
			7.47	-.017	0.867	7.50	-.018	0.829	7.47	-.012	1.192	7.51	-.015	0.975	
						20.30	-.008	0.683				21.34	-.004	1.177	
BLADE DRAG	1.78	-.117	0.530				1.81	-.115	0.531	1.76	-.083	0.751	1.81	-.117	0.522

TAB. 1 GRECA results - case F

	G.RE.CA.			FLIGHT TEST		
	Hz	c/cr	T/2	Hz	c/cr	T/2
LATERAL HUB	5.36	-.027	0.759	4.48	-.033	0.740
	5.88	-.019	0.985	5.89	-.020	0.953
	7.47	-.015	0.966	7.44	-.014	1.025
LONGITUDINAL HUB	4.53	-.017	1.437	4.42	-.037	0.671
	5.99	-.018	0.997	6.14	-.014	1.244
	7.47	-.012	1.191	7.14	-.010	1.495
BLADE DRAG	1.76	-.083	0.751	1.71	-.191	0.336

TAB 2 Compare GRECA results - flight tests (case F)
-- 75% airborne --

	G.RE.CA.			FLIGHT TEST		
	Hz	c/cr	T/2	Hz	c/cr	T/2
LATERAL HUB	3.91	-.056	0.504	4.85	-.044	0.514
	7.34	-.028	0.528	7.28	-.031	0.474
LONGITUDINAL HUB	3.91	-.035	0.800			
	5.90	-.019	0.956	5.94	-.021	0.857
	7.36	-.021	0.696	7.24	-.018	0.836
BLADE DRAG	1.78	-.117	0.530	2.33	-.104	0.456

TAB 3 Compare GRECA results - flight tests (case F)
-- 0% airborne --

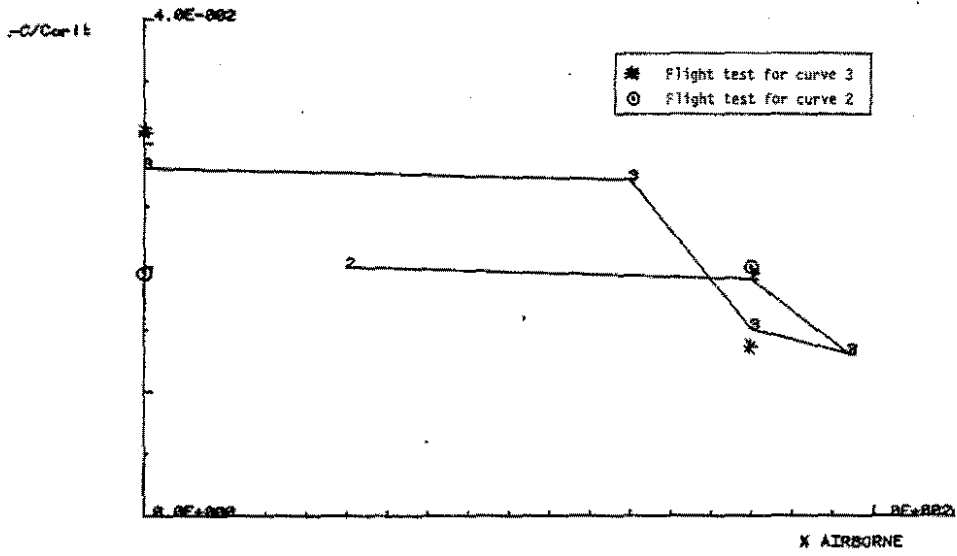


Fig. 17A Compare GRECA results - flight tests
 $-C/C_{orlt}$ versus X airborne - case F
 (LATERAL HUB DISPLACEMENT)

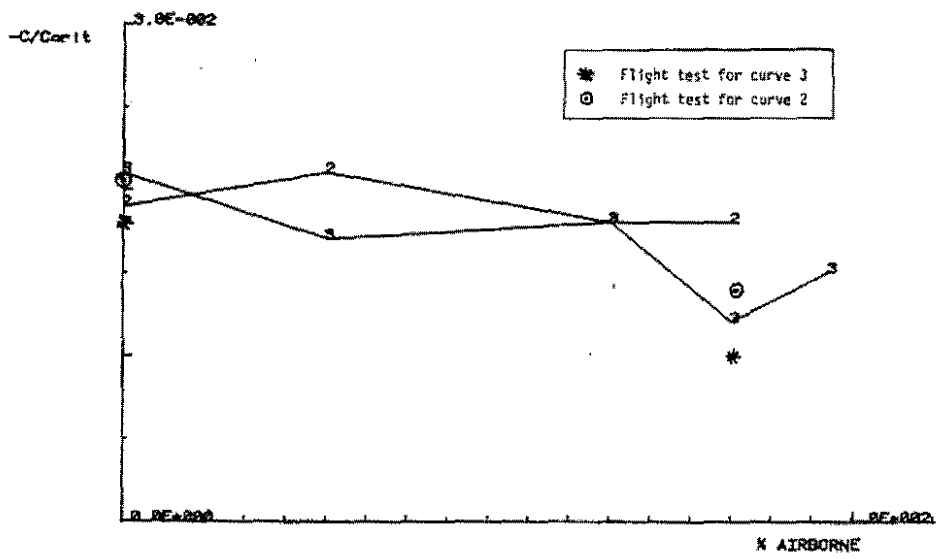


Fig. 17B Compare GRECA results - flight tests
 $-C/C_{orlt}$ versus X airborne - case F
 (LONGITUDINAL HUB DISPLACEMENT)

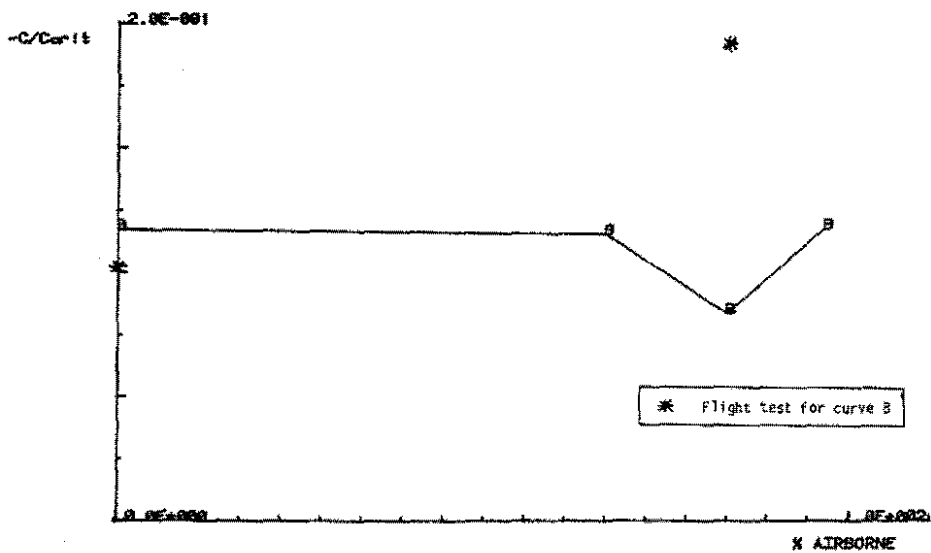


Fig. 17C Compare GRECA results - flight tests
 $-C/C_{orlt}$ versus X airborne - case F
 (BLADE DRAG MOTION)

6. CONCLUSIONS

A correct prediction of the dynamic behaviour of the helicopter on the ground before the first flight, is of fundamental importance for crew safety and to avoid all the negative effects arising from the possible destruction of the machine.

The paper presents the methodology followed by our company to reach this target. The basic idea was to develop a software able to accept the experimental data as soon as they become available. The final step is the utilization of the experimental results of the whole assembled system to reduce at a minimum level the simplified hypothesis

The experimental results carried out after the first flight seem to validate this approach whose further advantage is to follow the evolution of the results from the pre-design to the first flight.

7. REFERENCE

- 1) P. FRIEDMANN, C.E. HAMMOND, TZE-HSIN WOOD, Efficient numerical treatment of periodic systems with application to stability problems, International Journal for Numerical Methods in Engineering, vol. 11, 1117-1136(1977)
- 2) A. RUSSO, A. CERIOTTI, First results for the definition of a general rotorcraft dynamic program, meeting of Prediction of Aerodynamic Loads on Rotorcraft, Agard CPP-334, London 1982
- 3) W.G. BOUSMAN, D.J. WINKLER, Application of the Moving-Block Analysis
- 4) SDRC, Modal Plus Manual
- 5) G. SANSONE, Equazioni differenziali nel campo reale, Zanichelli Bologna, 1965
- 6) C.E. HAMMOND, An Application of Floquet Theory to Prediction of Mechanical Instability, Paper presented at AHS/NASA Ames Specialists' Meeting on Rotorcraft Dynamics, Feb. 1974
- 7) R. GABEL et al., Full Scale Ground and Air Resonance Testing of the Army-Boeing Vertol Bearingless Main Rotor, Paper presented at 35th Annual Forum of the AHS, May 1979

APPENDIX A

GROUND RESONANCE EQUATIONS OF MOTION

This appendix will utilize some concepts of the matrix algebra. To simplify the notation we will use the following convention:

- capital letters MATRIX (ex: A)
- small letters VECTOR (ex: y)
- small greek letter SCALAR (ex: α)

To deduce the Ground Resonance Equations we can start writing the equations of motion of the complete fuselage excited at the hub by the rotor forces (acting in the plane of the hub).

$$\begin{bmatrix} M_{HH}^* & M_{HF}^* \\ M_{FH}^* & M_{FF}^* \end{bmatrix} \begin{Bmatrix} \ddot{X}_H \\ \ddot{X}_F \end{Bmatrix} + \begin{bmatrix} C_{HH}^* & C_{HF}^* \\ C_{FH}^* & C_{FF}^* \end{bmatrix} \begin{Bmatrix} \dot{X}_H \\ \dot{X}_F \end{Bmatrix} + \begin{bmatrix} K_{HH}^* & K_{HF}^* \\ K_{FH}^* & K_{FF}^* \end{bmatrix} \begin{Bmatrix} X_H \\ X_F \end{Bmatrix} = \begin{Bmatrix} f_H \\ f_F \end{Bmatrix}$$

(1)

The subscript "H" stands for "hub" while "F" for fuselage;

- M^* = mass matrix
- C^* = damping matrix
- K^* = stiffness matrix
- f_H = force acting on the translational d.o.f. of the hub
- f_F = forces acting on any other d.o.f. of the fuselage
- x_H = hub d.o.f.
- x_F = fuselage d.o.f.

According to ref. 6, " f_H " can be deduced from the following matrix equation:

$$\begin{bmatrix} \overline{M}_{HH} & \overline{M}_{H\xi} \\ \overline{M}_{\xi H} & \overline{M}_{\xi\xi} \end{bmatrix} \begin{Bmatrix} \dot{X}_H \\ \dot{X}_\xi \end{Bmatrix} + \begin{bmatrix} \overline{c}_{HH} & \overline{c}_{H\xi} \\ \overline{c}_{\xi H} & \overline{c}_{\xi\xi} \end{bmatrix} \begin{Bmatrix} \dot{X}_H \\ \dot{X}_\xi \end{Bmatrix} + \begin{bmatrix} \overline{K}_{HH} & \overline{K}_{H\xi} \\ \overline{K}_{\xi H} & \overline{K}_{\xi\xi} \end{bmatrix} \begin{Bmatrix} X_H \\ X_\xi \end{Bmatrix} = \begin{Bmatrix} -f_H \\ \emptyset \end{Bmatrix} \quad (2)$$

where the sign "-" for f_H stands for "reaction" force, the superscript over the submatrices indicates the rotor and x_ξ = drag d.o.f..

The expanded form of the matrices of the equation (2) is:

$$[M] = \begin{bmatrix} \sum_1^{N_b} m_i & \emptyset & -S_{b_1} \sin \psi_1 & -S_{b_2} \sin \psi_2 & \dots & -S_{b_N} \sin \psi_N \\ \emptyset & \sum_1^{N_b} m_i & S_{b_1} \cos \psi_1 & S_{b_2} \cos \psi_2 & \dots & S_{b_N} \cos \psi_N \\ \hline -S_{b_1} \sin \psi_1 & S_{b_1} \cos \psi_1 & I_{b_1} & \emptyset & \dots & \emptyset \\ -S_{b_2} \sin \psi_2 & S_{b_2} \cos \psi_2 & \emptyset & I_{b_2} & \dots & \emptyset \\ \vdots & \vdots & \vdots & \vdots & \ddots & \vdots \\ -S_{b_N} \sin \psi_N & S_{b_N} \cos \psi_N & \emptyset & \emptyset & \dots & I_{b_N} \end{bmatrix}$$

$$[c] = \begin{bmatrix} \emptyset & \emptyset & -2S_{b_1} \Omega \cos \psi_1 & -2S_{b_2} \Omega \cos \psi_2 & \dots & -2S_{b_N} \Omega \cos \psi_N \\ \emptyset & \emptyset & -2S_{b_1} \Omega \sin \psi_1 & -2S_{b_2} \Omega \sin \psi_2 & \dots & -2S_{b_N} \Omega \sin \psi_N \\ \hline \emptyset & \emptyset & c_{b_1} & \emptyset & \dots & \emptyset \\ \emptyset & \emptyset & \emptyset & c_{b_2} & \dots & \emptyset \\ \vdots & \vdots & \vdots & \vdots & \ddots & \vdots \\ \emptyset & \emptyset & \emptyset & \emptyset & \dots & c_{b_N} \end{bmatrix} \quad (3)$$

$$[K] = \begin{bmatrix} \emptyset & \emptyset & S_{b_1} \Omega^2 \sin \psi_1 & S_{b_2} \Omega^2 \sin \psi_2 & \dots & S_{b_n} \Omega^2 \sin \psi_n \\ \emptyset & \emptyset & -S_{b_1} \Omega^2 \cos \psi_1 & -S_{b_2} \Omega^2 \cos \psi_2 & \dots & -S_{b_n} \Omega^2 \cos \psi_n \\ \hline \emptyset & \emptyset & (K_{b_1} + \Omega^2 e S_{b_1}) & \emptyset & \dots & \emptyset \\ \emptyset & \emptyset & \emptyset & (K_{b_2} + \Omega^2 e S_{b_2}) & \dots & \emptyset \\ \emptyset & \emptyset & \emptyset & \emptyset & \dots & (K_{b_n} + \Omega^2 e S_{b_n}) \end{bmatrix} \quad (3)$$

- m_i = mass of the i-th blade
 S_{b_i} = Static moment of the i-th blade
 I_{b_i} = Mass moment of inertia of the i-th blade
 C_{b_i} = Damping coefficient of the i-th blade
 Ω = angular velocity of the rotor
 K_{b_i} = Elastomeric cocking stiffness of the i-th blade
 e = Drag hinge offset

Substituting the equation (2) into (1) and combining the equations of motion of the blades we obtain the **ground resonance equations**, leaving in evidence the contribution of the fuselage and of the rotor:

$$\begin{bmatrix} M_{HH}^* & M_{HF}^* & \emptyset \\ M_{FH}^* & M_{FF}^* & \emptyset \\ \hline \emptyset & \emptyset & \emptyset \end{bmatrix} \ddot{X} + \begin{bmatrix} \bar{M}_{HH} & \emptyset & \bar{M}_{HF} \\ \emptyset & \emptyset & \emptyset \\ \hline \bar{M}_{FH} & \emptyset & \bar{M}_{FF} \end{bmatrix} \ddot{X} + \\
 \begin{bmatrix} C_{HH}^* & C_{HF}^* & \emptyset \\ C_{FH}^* & C_{FF}^* & \emptyset \\ \hline \emptyset & \emptyset & \emptyset \end{bmatrix} \dot{X} + \begin{bmatrix} \bar{C}_{HH} & \emptyset & \bar{C}_{HF} \\ \emptyset & \emptyset & \emptyset \\ \hline \bar{C}_{FH} & \emptyset & \bar{C}_{FF} \end{bmatrix} \dot{X} + \\
 \begin{bmatrix} K_{HH}^* & K_{HF}^* & \emptyset \\ K_{FH}^* & K_{FF}^* & \emptyset \\ \hline \emptyset & \emptyset & \emptyset \end{bmatrix} X + \begin{bmatrix} \bar{K}_{HH} & \emptyset & \bar{K}_{HF} \\ \emptyset & \emptyset & \emptyset \\ \hline \bar{K}_{FH} & \emptyset & \bar{K}_{FF} \end{bmatrix} X = \emptyset \quad (4)$$

$x = x_H, x_F, x^T$ d.o.f. vector.

If we want to use directly the results of the experimental tests (ref. 4) it is necessary to introduce the modal d.o.f. of the fuselage; the transformation matrix is:

$$\begin{Bmatrix} X_H \\ X_F \\ X_f \end{Bmatrix} = \begin{bmatrix} \Phi_F & \emptyset \\ \emptyset & I \end{bmatrix} \begin{Bmatrix} X_m \\ X_f \end{Bmatrix} \quad (5)$$

Φ_F = modal matrix of the fuselage
 x = modal d.o.f. of the fuselage

So with this new set of d.o.f. we finally obtain:

$$\begin{bmatrix} M_F^* & \emptyset \\ \emptyset & \emptyset \end{bmatrix} \begin{Bmatrix} \ddot{X}_m \\ \ddot{X}_f \end{Bmatrix} + \begin{bmatrix} \Phi_F^T \bar{M}_{11} \Phi_F & \Phi_F^T \bar{M}_{12} \\ \bar{M}_{21} \Phi_F & \bar{M}_{22} \end{bmatrix} \begin{Bmatrix} \ddot{X}_m \\ \ddot{X}_f \end{Bmatrix} +$$

$$\begin{bmatrix} C_F^* & \emptyset \\ \emptyset & \emptyset \end{bmatrix} \begin{Bmatrix} \dot{X}_m \\ \dot{X}_f \end{Bmatrix} + \begin{bmatrix} \emptyset & \Phi_F^T \bar{C}_{12} \\ \emptyset & \bar{C}_{22} \end{bmatrix} \begin{Bmatrix} \dot{X}_m \\ \dot{X}_f \end{Bmatrix} +$$

$$\begin{bmatrix} K_F^* & \emptyset \\ \emptyset & \emptyset \end{bmatrix} \begin{Bmatrix} X_m \\ X_f \end{Bmatrix} + \begin{bmatrix} \emptyset & \Phi_F^T \bar{K}_{12} \\ \emptyset & \bar{K}_{22} \end{bmatrix} \begin{Bmatrix} X_m \\ X_f \end{Bmatrix} = \emptyset \quad (6)$$

The equations written in the physical d.o.f. (4) or in the modal form (6) are also used in the design phase, utilizing the analytical results of non-linear finite element programs.

APPENDIX B

INTEGRATION SCHEME

This appendix will utilize the same convention described in Appendix A to represent the matrix expression.

The computation of the "FLOQUET TRANSITION MATRIX" take advantage from the theory developed by PEANO, described in ref. 5, where the solution of a system of differential omogeneous equations, with constant coefficients:

$$\dot{y} = A*y \quad (1)$$

where:

A = matrix of constant coefficients which expression for a dynamic system is

$$A = \left[\begin{array}{c|c} -M^{-1}*B & -M^{-1}*K \\ \hline U & 0 \end{array} \right]$$

M = mass matrix

B = damping matrix

K = stiffness matrix

U = unity matrix

y = $\{\dot{y}, y\}^T$ vector of velocities and displacements,

can be obtained resolving the following equation

$$y(t) = e^{At}*y_0 \quad (2)$$

where:

e = base of the natural logarithm

$$e^{At} = \sum_0^{\infty} (A^i*t^i)/i! \quad (3)$$

$A^i = A*A*...A$ "i" times; and $A^0 = U$

$y_0 = \{\dot{y}_0, y_0\}^T$ any starting value of velocities and displacements

$y(t) = \{\dot{y}(t), y(t)\}^T$ solution at the desired time "t"

The Eq.(3) provides the method to compute, with the desired approximation, the integration matrix. Each term of the series can be obtained from the previous one according to the relation:

$$((At)^{r+1})/(r+1)! = (At)^r/(r!)*(At)/(r+1) \quad (4)$$

From the matrix theory the Eq.(1) can be written as

$$\dot{y} = \phi_A * L * \phi_A^{-1} * y \quad (5)$$

where:

ϕ_A = matrix containing in each column the eigenvectors of the matrix "A"

L = diagonal matrix containing in the same order, the eigenvalues of "A".

From the Eq.(3) the integration matrix becomes:

$$\begin{aligned} e^{At} &= \phi_A * e^{\lambda t} * \phi_A^{-1} \\ &= \phi_A * P * \phi_A^{-1} \end{aligned} \quad (6)$$

where:

$e^{\lambda t} = P =$ diagonal matrix.

The relation between the characteristic exponents of the matrix "P" and the eigenvalues λ , using the rules of the imaginary numbers as:

$$\lambda_{\pi} = \alpha_{\pi} + i \beta_{\pi}$$

$$\lambda_{p\pi} = \pi\tau + i\omega_{\pi}$$

is:

$$\alpha r = \frac{1}{2t} * \lg (\pi r^2 + \omega r^2) \quad (7)$$

$$\beta r = \frac{1}{t} * \operatorname{atg} (\omega r / \pi r) + n \pi \quad (8)$$

(n to be determined).

The system (2) is stable when:

$$\lim_{t \rightarrow \infty} y(t) = 0$$

This happens when:

$$\lim_{t \rightarrow \infty} e^{\lambda t} = 0$$

That is when the real part of all the eigenvalues " λ " are negative or identically, when all the modules of the characteristic exponents are less than unity (Eq.(7)).

If the coefficients of the matrix "A" are function of time, the solution of the system (1) can be approximatively computed considering the coefficients of "A" constant step by step. Thus:

$$\begin{aligned} \bar{y}(t_1) &= e^{A_0 * \delta t_1} * y_0 \\ \bar{y}(t_2) &= e^{A_1 * \delta t_2} * y(t_1) \\ &\dots\dots\dots \\ \bar{y}(t) &= e^{A_{n-1} * \delta t_n} * y(t_{n-1}) \end{aligned} \quad (9)$$

where " A_j " can be computed in any desired time between t_{j+1} and t_j according to Eq.(3).

The value of the solution, as a function of the initial condition " y_0 ", is then:

$$\begin{aligned} \bar{y}(t) &= (e^{A_{n-1} * \delta t_n} * \dots * e^{A_0 * \delta t_1}) * y_0 \\ &= \left(\prod_{j=0}^{n-1} e^{A_j * \delta t_{(j+1)}} \right) * y_0 \end{aligned} \quad (10)$$

$$\bar{y}(t) = \bar{R} * y_0$$

Considering " δt " constant its value can be expressed by:
 $\delta t = t/n$.

Then the exact value of the solution can be deduced from:

$$y(t) = \lim_{n \rightarrow \infty} \left(\prod_{j=0}^n e^{A_j * t/n} \right) * y_0 \quad (11)$$

$$= R * y_0$$

In the case where "A" has constant coefficients the above equation reduces to Eq.(2).

The stability concept can not be applied for this kind of differential equations and the only way to understand its asymptotic behaviour is to follow the results of the integration.

The computation of the matrix "R(t)" can be carried out either through the repeated use of the Eq.(3), or utilizing any integration scheme, observing that each column of the matrix "R" coincide with the solution y(t) that we obtain perturbing unically the corresponding initial conditions with an intensity equal to one (Eq.(11)). Any desired intensity can, otherwise be utilized as the solution, for the linearity of the system, will be modified of the same amount.

In the case where the matrix "A" has periodic coefficients, after any their cycle "T", the sequence of operations described from Eq.(9) to Eq.(11) repeat themselves i.e.:

$$y(T) = R_T * y_0$$

$$y(2T) = R_T * y(T) \quad (12)$$

.....

$$y(nT) = R_T * y((n-1)T)$$

or

$$y(nT) = (R_T)^n * y_0 \quad (13)$$

The system with periodic coefficient behaves so, like a system with constant coefficients where the role of the matrix e^{AT} is played by the constant matrix " R_T " called in this case: THE FLOQUET TRANSITION MATRIX.

We are so able to know the solution at the end of each period of variation of the coefficients and then of its asymptotic behaviour.

The signal obtained with the help of the "TRANSITION MATRIX" will result an envelope of the actual signal and the frequencies greater than the FLOQUET FREQUENCY, will then be affected by the aliasing phenomenon. This is the main reason for the indetermination contained in Eq.(8).

The stability of a differential system with periodic coefficient is thus determined unically from the matrix " R_T " and typically from the results after periods.

The system is stable when :

$$\lim_{n \rightarrow \infty} y(nT) = 0$$

that is when the eigenvalues of " R_T " matrix have modulus less than one like Eq.(7).